Search for GeV γ-Ray Pair Halos Around Low Redshift Blazars

Wenlei Chen,* James H. Buckley, and Francesc Ferrer
Department of Physics and McDonnell Center for the Space Sciences, Washington University in St. Louis, St. Louis, Missouri 63130, USA

(Received 28 October 2014; revised manuscript received 15 October 2015; published 16 November 2015)

We report on the results of a search for γ-ray pair halos with a stacking analysis of low redshift blazars using data from the Fermi Large Area Telescope. For this analysis we used a number of *a priori* selection criteria, including the spatial and spectral properties of the Fermi sources. The angular distribution of $\sim$1 GeV photons around 24 stacked isolated high-synchrotron-peaked BL Lacs with redshift $z < 0.5$ shows an excess over that of pointlike sources. A frequentist test yields a p value of $p \sim 0.01$ for the extended emission against the point-source hypothesis. A Bayesian estimation provides Bayes factors $\log_{10} B_{10} > 2$, consistent with expectations for pair halos produced in the intergalactic magnetic fields with strength $B_{\mathrm{IGMF}} \sim 10^{-17}$–$10^{-15}$ G.

DOI: 10.1103/PhysRevLett.115.211103 PACS numbers: 95.85.Pw, 98.54.Cm, 98.58.Ay, 98.80.Es

Introduction.—The magnetic fields that are observed in galaxies and galaxy clusters are believed to result from the dynamo amplification of weak magnetic field seeds, whose origin remains a mystery. Intergalactic magnetic fields (IGMFs), deep in the voids between galaxies, provide the most accurate image of the weak primordial seed fields and could be linked to the early stages in the evolution of the Universe (see, e.g., [1] for a recent review). Among the several methods used to study cosmological magnetic fields (see, e.g., [2] for a recent review), the observation (or nondetection) of cascade emission from blazars can potentially measure very weak IGMFs. A number of blazars have been observed to emit both very-high-energy (VHE, > 100 GeV) γ rays with ground-based γ-ray instruments and high-energy (MeV/GeV) γ rays with the Fermi Gamma-Ray Space Telescope [3,4]. Most of the detected TeV γ rays are from the nearest sources since such high-energy γ rays cannot propagate over long distances in intergalactic space due to interactions with the extragalactic background light (EBL). Of course, some higher-redshift sources still have detectable TeV emission (e.g., blazar PKS1424 + 240, which has redshift lower limit of $z > 0.6$ [5]), but with highly absorbed spectra consistent with theoretical calculations of the attenuation by the EBL [6–10]. These interactions of TeV γ rays with the EBL produce electron-positron pairs that subsequently are cooled by inverse Compton (IC) interactions with the cosmic microwave background (CMB), ultimately leading to GeV γ-ray emission from these pair cascades. Since magnetic fields deflect the electron-positron pairs changing the angular distribution of cascade emission, searches for extended GeV emission around blazars can provide an avenue for constraining the IGMF.

Because of the low GeV γ-ray flux from extragalactic sources, it is difficult to examine the angular extent of the photon events from a single blazar or even to assess the joint likelihood for detailed fits to a set of individual sources where individual source parameters are taken to be completely independent. To overcome this limitation, stacking sources has been used to make such statistical analysis feasible. Despite early hints at a signal in the stacking analysis of 170 brightest active galactic nuclei (AGNs) using 11-month Fermi observations [11], by comparing with the GeV emission from the Crab Nebula [which is essentially a point source for the Fermi Large Area Telescope (Fermi-LAT)], A. Neronov *et al.* [12] found no significant evidence of extended emission and argued that the apparent excess could be attributed to an underestimation of the real point-spread function (PSF) [13]. A subsequent analysis by Ackermann *et al.* [14] comparing an updated PSF to 100 stacked BL Lac AGNs did not find any statistically significant halo emission either.

The cascade emission from individual blazars has also been studied by modeling the intrinsic TeV spectra and adopting EBL and CMB models (e.g., [15–19]). Delays in arrival time of the cascade emission were used to explain the nondetection of several TeV sources in Fermi energy, and to derive a lower bound of the IGMF strength (e.g., $\sim 10^{-20}$–10^{-19} G in [15]). The angular extent of the cascade signals caused by IGMFs above $\sim 10^{-16}$ G also provided an explanation for the nondetection of TeV sources 1ES 0229 + 200 and 1ES0347-121 by Fermi [16]. W. Essey *et al.* reported a possible *measurement* of IGMFs in the range 1×10^{-17}–3×10^{-14} G [17] based on the TeV–GeV spectra. Very recently, a study of 1ES0347-121 spectral energy distribution provided an IGMF estimation of 3×10^{-17} G [19]. Fitting to TeV data from, e.g., VERITAS and HESS, such studies yielded detailed predictions of the cascade emission, but invariably made assumptions about the sources, e.g., the relationship of the long-term TeV emission to the measurement of a few flares. The upper bound of the IGMF strength with correlation length above $\sim$1 Mpc is below $\sim 10^{-9}$ G constrained by the nondetection of the large scale CMB anisotropies, and is given to be $\sim 10^{-12}$ G by the

TABLE I. Energy bins and values of $\theta_{\rm in}$.

Energy (GeV)	1–1.58	1.58–3.16	3.16–10	10–100
$\theta_{\rm in}$	2.3°	1.6°	1°	0.8°

galaxy cluster simulation, as summarized in [16,20]. The likely range of the IGMF strength from previous studies is given from $\sim 10^{-20}$ to $\sim 10^{-12}$ G.

As the energies of the primary γ rays increase, the pair production occurs closer to the source, reducing the angular size of the cascade. Depending on the strength of the IGMF and the redshift of the source, the highest energy emission might not be resolved by the Fermi PSF. While at lower energies (especially for the nearest sources), the emission may be too diffuse to be readily detected. It follows that only a few blazars would have cascade emission that can be statistically detected through their angular profiles.

In our study, we combine data from 24 isolated high-synchrotron-peaked (HSP) BL Lacs which are *a priori* selected to provide the best prospects for detection and adequate photon counting statistics. A frequentist likelihood ratio test (LRT) is applied to provide the pair-halo detection significance. Bayes factors are further evaluated to estimate the pair-halo parameters (the angular size and halo fraction), providing the possible range of IGMF strength.

Data preparation and selection criteria for stacking sources.—We use the Fermi-LAT Pass 7 reprocessed data through February 2014: SOURCE class front-converted photon events are binned into four logarithmically spaced energy ranges to roughly equalize counts (see Table I). The source candidates are selected from the AGN associated sources in the Fermi-LAT High-Energy Catalog [4]. The regions of the Galactic disk and Fermi bubbles are excluded to avoid anisotropic background emission [21].

Data are also divided into angular bins to provide adequate statistics. Source bins of an equal solid angle are set around the direction of the source, surrounded by a larger background bin with an outer boundary of 5°. To reduce systematic errors from nearby sources, we require that no nearby sources (those bright enough to appear in the LAT 2-year Point Source Catalog [3]) are within 2.3° of the stacked sources and correct for the impact of any remaining nearby sources by defining an exclusion region of radius $\theta_{\rm cut}$ (= 2.3°) about these sources; we account for these exclusion regions by assuming that the signal and background effective area is reduced in proportion to the excluded solid angle. The size of the source bins $\theta_{\rm in}$ is a function of energy chosen to be greater than the 95% containment angle of the PSF in the corresponding energy range [27] (see Table I).

Assuming that the correlation length of the IGMF is much greater than the mean free path for IC scattering ($\sim 10^1$–10^2 kpc, see detailed discussion in [20], also in [28]), we estimate the typical size of a pair halo to be

$$\Theta(E_\gamma, z_s, B_0) \approx 9.2 \times 10^{-4}[1 + z_{\gamma\gamma}(E_\gamma, z_s)]^{-2} \times \left(\frac{E_\gamma}{100\ \text{GeV}}\right)^{-1}\left(\frac{B_0}{10^{-16}\ \text{G}}\right)\left[\frac{d_\gamma(E_\gamma, z_s)}{d_s(z_s)}\right], \quad (1)$$

where E_γ is the energy of the cascade photon observed by Fermi, z_s is the observed redshift of the source, and B_0 is the field strength at the present epoch. To get the estimate above, we followed the discussion in Neronov and Semikoz [20] (see also [28]), where $z_{\gamma\gamma}$ is the redshift of pair production, and d_γ and d_s are the comoving mean free path for pair production and the comoving distance to the source, respectively [21]. Given the finite Fermi PSF, detecting the extended emission from high-redshift sources is quite unlikely. For example, from Eq. (1), an IGMF of $\sim 10^{-16}$ G would result in a halo of angular radius of ∼2° at 1 GeV for a source at $z = 0.3$. If the same source was located at $z = 0.8$, the halo size would decrease to ∼0.2°, which is much smaller than the Fermi PSF and would appear like a point source. In addition, most of the sources from $z < 0.5$ would be seen along the lines of sight that do not cross astrophysical systems (i.e., galaxy and galaxy clusters) which host large magnetic fields [6], indicating that the cascade emission from these sources is most likely produced in intergalactic space.

Both observational and theoretical arguments lead us to expect that HSP BL Lac objects are the most likely sources of the VHE γ rays needed to produce the GeV cascades. For example, in [29,30], we see a strong correlation of the occurrence of a HSP energy with TeV emission. This is naturally explained if the same population of VHE electrons that produces the X-ray synchrotron radiation also produces the TeV γ rays by IC in the source region (e.g., AGN jets). For this study, we subdivide data into flat spectrum radio quasars (FSRQs), and BL Lac objects. Since the FSRQs are typically very distant sources with lower-energy synchrotron peaks, we expect these sources to lack observable GeV pair halos, serving as a control population.

Distribution of the GeV γ rays around stacked blazars.—We identify 24 HSP BL Lacs with redshift $z < 0.5$ that satisfy our selection criteria and stack their photon events. As a control population, 26 FSRQs (with any redshift) are also selected by the same criteria. As evident in past searches for pair halos, a thorough understanding of the PSF is critical for this type of study. Pulsars with unresolved pulsar wind nebulae can be used as calibration sources since they are effective point sources for Fermi-LAT [12,14]; here we choose the Geminga [31] and Crab [32] pulsars. To plot different angular distribution profiles of different stacked source classes, we calculate and remove the diffuse background for each source, sum the background-subtracted counts, and then normalize the profiles. We calculate the angular profiles for the stacked pulsars, the 24 BL Lacs, and the 26 FSRQs, as shown in Fig. 1. The angular profiles for stacked pulsars agree with their PSFs (P7REP_SOURCE_V15) in each energy range [21]. The normalized angular profiles of stacked BL Lacs have lower scaled counts per unit

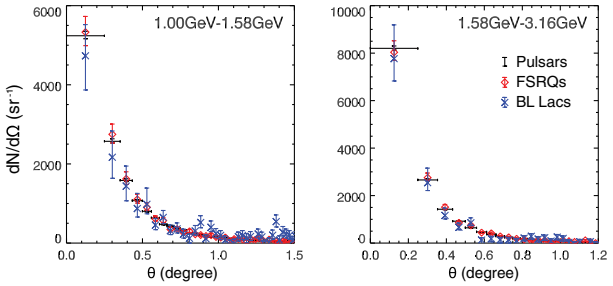

FIG. 1 (color online). Angular distribution of photon events around the stacked pulsars (black), the stacked FSRQs (red), and the stacked BL Lacs (blue): vertical errors are the 68% confidence intervals; horizontal errors show the size of angular bins.

solid angle at small θ, providing evidence for extended emission since the additional counts in the extended halo reduce the scaled counts at small angles after normalization. The deficit in counts at small θ (evidence for extended emission) is only significant in the lowest energy bin, consistent with the expectation that the angular extent of the halo is larger at lower energies, as indicated in Eq. (1). In contrast, the angular profiles of the stacked FSRQs are indistinguishable from our surrogate point-source data from pulsars, as shown in Fig. 1.

Statistical evidence for pair-halo emission and estimation of the IGMF.—To model the normalized angular profiles $g(\theta)$, we use

$$g(\theta; f_{\rm halo}, \Theta) = f_{\rm halo} g_{\rm halo}(\theta; \Theta) + (1 - f_{\rm halo}) g_{\rm psf}(\theta), \quad (2)$$

where $f_{\rm halo}$ is the fraction of the pair-halo component, and Θ is a single parameter characterizing the angular extent of the halo. $g_{\rm psf}(\theta)$ is the effective PSF for the stacked source [21] and $g_{\rm halo}(\theta; \Theta)$ is a Gaussian function of θ (in the small-angle approximation) convolved with the PSF. Then, the number of photon events in the jth angular bin around the stacked source is estimated by

$$\lambda_j(f_{\rm halo}, \Theta, \boldsymbol{\mu}, \boldsymbol{A}) = \sum_i (A_i g_j + \mu_i) \Omega_{i,j} w_{i,j}, \quad (3)$$

where g_j is the discrete value of the normalized angular distribution $g(\theta)$ given by Eq. (2), and $\boldsymbol{A}$ and $\boldsymbol{\mu}$ are a set of normalization factors $\{A_i\}$ and a set of the assumed uniform background values (in counts per unit solid angle) $\{\mu_i\}$, respectively, for each source i. $\Omega_{i,j}$ is the solid angle of the jth angular bin around the ith source. $w_{i,j} = \mathcal{E}_{i,1}/\mathcal{E}_{i,j}$ is the exposure corrector to calibrate the expected counts in the jth angular bin around the ith source to the level of the center angular bin of this source, where $\mathcal{E}$ is the averaged exposure of the angular bin. For a given configuration of the angular bins, a set of estimators $\{\lambda_j\}$ is a function of $f_{\rm halo}$, Θ, $\boldsymbol{\mu}$, and $\boldsymbol{A}$.

We present both a frequentist *test* and a Bayesian *estimation* of the data. A set of observed counts $\boldsymbol{N} = \{N_{i,j}\}$ are estimated by the model given by Eq. (3), where $N_{i,j}$ is the number of counts in the jth angular bin around the ith source. Counts in the background bins are also estimated by the isotropic background model derived from $\boldsymbol{\mu}$. For the frequentist analysis, the maximum likelihood estimation (MLE) is used for the model fitting. The logarithm of the likelihood ratio is evaluated as a test statistic (TS), providing the confidence level of getting $\boldsymbol{N}$. A simple application of a full maximum likelihood method requires that we introduce free parameters $\{A_i\}$, $\{\mu_i\}$ describing the independent normalization factors and background parameters for each source. In principle, the best fit parameters can then be found by simultaneously maximizing the joint likelihood function $\mathcal{L} \equiv \prod_{i,j} P(N_{i,j}|\lambda_{i,j})$ with respect to $\{A_i\}$, $\{\mu_i\}$ and parameters describing the effective halo fraction and angular extent. However, the small number of counts in each source or angular bin $\{N_{i,j}\}$ and the large set of (nonidentical) probability distributions results in a nonconverging distribution of the TS, and both a procedural problem in finding the global maximum. While this is addressed by the Bayesian analysis, it is problematic for a frequentist inference [33]. Here we adopt a novel approach [21] where we repartition the data into two sets: the stacked angular distribution $\{\sum_{i=1}^{n} N_{i,j}\} \equiv \{\eta_j\}$ obtained by summing over sources i, and the stacked source distribution $\{\sum_{j=1}^{m} N_{i,j}\} \equiv \{\zeta_i\}$ obtained by summing over angular bins j, where m and n are the total number of angular bins and stacked sources, respectively. The likelihood of obtaining $\{\zeta_i\}$ and $\{\eta_j\}$ is calculated as $\mathcal{L}_{\rm on}$. This is combined with the likelihood of getting a set of $\{N_{i,m}\}$ counts detected in each background bin around each source $\mathcal{L}_{\rm off}$.

We subsequently evaluate the joint likelihood $\mathcal{L} = \mathcal{L}_{\rm on} \times \mathcal{L}_{\rm off}$ which is defined in the multidimensional space of the model parameters, $\boldsymbol{x} = (f_{\rm halo}, \Theta, \boldsymbol{\mu}, \boldsymbol{A})$ [21]. Note that both ζ_i and η_j have relatively large numbers of counts, and $N_{i,m}$ is also relatively large since the solid angle of the background bins is much larger than that of an individual angular bin (i, j); hence, the following frequentist analysis acting on ζ_i, η_j, and $N_{i,m}$ will not encounter the problem of small sample size. To get the quantitative significance of the pair halo, we focus on the space of the two model parameters, $f_{\rm halo}$ and Θ. We must distinguish between two hypotheses in this space: the hypothesis of halo emission $\mathcal{H}_1$ and the null hypothesis $\mathcal{H}_0$, where $\mathcal{H}_0$ denotes a pure point source where either $f_{\rm halo} = 0$ or $\Theta = 0$, and for $\mathcal{H}_1$, the two parameters are free. The ratio of the maximum likelihood of $\mathcal{H}_1$ for a given pair of $f_{\rm halo}$ and Θ to that of $\mathcal{H}_0$ is evaluated and displayed in $(f_{\rm halo}, \Theta)$ space. Figure 2 shows the likelihood ratio maps for the stacked BL Lacs (a) and the maps for the simulated point source (labeled PSF) with total number of events in each energy bin set to that of the stacked BL Lacs (b). From Eq. (2), $\mathcal{H}_0$ gives $g(\theta) = g_{\rm psf}(\theta)$, indicating that any point on $f_{\rm halo}$ and Θ axes in each map gives a constant likelihood corresponding to a null model without extended emission. Figure 2(b) shows that the maximum values of the likelihood ratio are distributed along the axes, consistent with the null hypothesis.

The 1–1.58 GeV likelihood ratio map shows a peak at nonzero $f_{\rm halo}$ and Θ (Fig. 2). In the higher energy bins [21], the highest likelihood appears close to the $f_{\rm halo}$ and Θ axes (where the null model is located). The fact that the likelihood maps for the higher energy bins are consistent

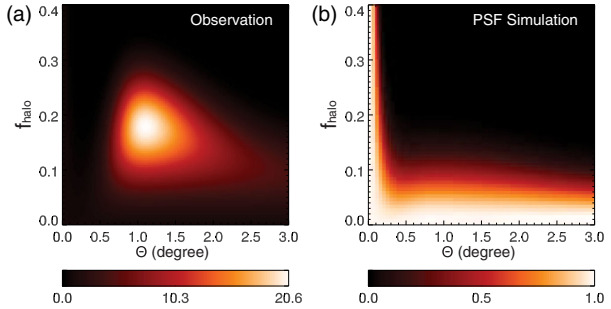

FIG. 2 (color online). Likelihood ratio maps in the 1–1.58 GeV energy bin. Colors show the ratio of the likelihood of the extended-emission hypothesis to that of the null hypothesis (the PSF). (a) Likelihood ratio maps for stacked BL Lacs. (b) Likelihood ratio maps for a point source with angular distribution given by the PSF and with total number of events in each energy bin set equal to that of the stacked BL Lacs.

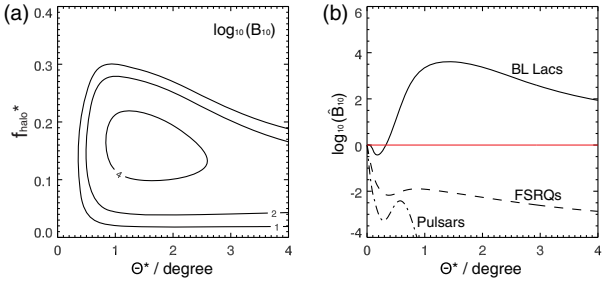

FIG. 3 (color online). Bayes factors in the 1–1.58 GeV energy bin. (a) Bayes factors of the hypotheses $H_1(f_{\rm halo} = f^*_{\rm halo}, \Theta = \Theta^*)$ against $\mathcal{H}_0(\{f_{\rm halo} = 0\} \bigcup \{\Theta = 0\})$ for the stacked BL Lacs. (b) Bayes factors of the hypotheses $\hat{H}_1(f_{\rm halo} \in (0, 1], \Theta = \Theta^*)$ against $\mathcal{H}_0$ for the stacked BL Lacs (solid line), FSRQs (dashed line), and pulsars (dash-dot line).

with the null hypothesis matches our expectation based on the angular distribution measurements shown in Fig. 1, where no significant difference is seen between the profiles of stacked pulsars and stacked BL Lacs in the plots of the higher energy bins. From the distributions of the maximum values of the likelihood ratio, the pulsars are shown to appear as point sources for Fermi-LAT [21]. We simulated the distribution of the TS by using a Monte Carlo method based on the null hypothesis. The LRT shows that if the stacked source appears to be a point source given by the Fermi PSF, the significance (p value) of the observation in the 1–1.58 GeV energy bin is $p \sim 0.01$, equivalent to the significance of a normal distributed sample at $\sim 2.3\sigma$ [21].

We calculate the Bayes factors $B_{10} = \mathcal{L}_B(H_1|\boldsymbol{N})/\mathcal{L}_B(\mathcal{H}_0|\boldsymbol{N})$ [34,35] of the extended-emission hypothesis H_1 for given values of $f_{\rm halo} = f^*_{\rm halo}$ and $\Theta = \Theta^*$ (a subset of $\mathcal{H}_1$) against the null hypothesis $\mathcal{H}_0$ [21]. For hypotheses $\boldsymbol{H} = \{\mathcal{H}_0, H_1\}$, the Bayesian likelihood $\mathcal{L}_B$ is given by

$$\mathcal{L}_B(\boldsymbol{H}|\boldsymbol{N}) = \int d\boldsymbol{x} P(\boldsymbol{N}|\boldsymbol{x}, \boldsymbol{H}) \pi(\boldsymbol{x}|\boldsymbol{H}). \quad (4)$$

Different from the frequentist LRT, for a Bayesian method, the problem of limited statistics in the (i, j) bins is eliminated [33], and we can include all the information contained in the data. We are left with the straightforward (but computationally difficult) task of evaluating the multidimensional integral over model parameters to obtain the p value. In Eq. (4), the prior can be designed to constrain the total number of counts with no additional assumptions, while the posterior density is given by the joint Poisson likelihood of getting the observation $\boldsymbol{N}$ [21].

We plot the contours of $\log_{10} B_{10}$ in the $f^*_{\rm halo}$-Θ^* coordinates, as shown in Fig. 3(a). Taking $\log_{10}(B_{10}) > 2$ (referred to as "decisive" evidence by [34]), we find the signal in the 1–1.58 GeV energy bin to favor the hypothesis of extended emission against the null hypothesis. While $\log_{10}(B_{10}) < 0.5$ at higher energies, providing no significant evidence against the null hypothesis. To estimate the IGMF, we focus on the model factor Θ, and seek to get the quantitative significant range of its values for the stacked BL Lacs. We introduce a hypothesis $\hat{H}_1$ for a given Θ^* with all possible values of $f_{\rm halo}$. The Bayes factors of $\hat{H}_1$ can be evaluated by integrating the Bayesian likelihood $\mathcal{L}_B$ over all possible values of $f_{\rm halo}$ [21]. Thus, the resulting Bayes factors $\hat{B}_{10}$ of $\hat{H}_1$ against $\mathcal{H}_0$ are given as a function of Θ^*, as shown in Fig. 3(b). From the Bayes factors, we obtain the values of Θ given by the most likely hypothesis [where $\log_{10}(\hat{B}_{10}) > 2$]: $\sim 0.6°$–$4°$ in the first energy bin. Recalling Eq. (1), using the average redshift of the stacked BL Lacs $\langle z \rangle \approx 0.23$, the strength of IGMF is conservatively estimated to be in the range of $B_{\rm IGMF} \sim 10^{-17}$–$10^{-15}$ G. These values are larger than the lower bound derived from observations of 1ES0347-121 in [16] and consistent with the results in [11,17,19]. The negative Bayes factors for the stacked pulsars and FSRQs [as shown in Fig. 3(b)] provide no evidence for pair halos, consistent with the results given by the frequentist LRT.

To use our Bayesian analysis to determine the significance of the detection, we need to integrate the priors for both the halo fraction and angular extent. For the halo fraction, this is straightforward (as discussed above), resulting in the projected Bayes factor $\hat{B}_{10}$. But, determining a prior probability for the halo extent is more difficult since our method is only sensitive to angular extents up to a few degrees (because of the finite search window), while IGMF values as large as 10^{-9} G would result in halos covering the whole sky. To phrase the result in the more familiar language of frequentist statistics, by not explicitly integrating over the prior in Θ we incur a *trials factor* in interpreting the Bayes factor as the significance of detection of pair halos. However, since $\log_{10}(\hat{B}_{10}) > 2$ over most of the explored parameter space, this trials factor is small and we can qualitatively interpret the results as providing evidence for halo emission.

Discussion.—In this study, we presented an analysis of the angular distribution of γ rays from a subset of sources selected *a priori* to minimize systematics but maximize chances of finding spatially resolved halo emission. This study provides an interesting hint of a detection of pair halos, shown both by a frequentist and a Bayesian analysis, resulting in a possible measurement of the IGMF, consistent with prior limits.

Most of the Fermi sources have nearby sources (within 2°), which will contaminate the stacked angular profiles. Previous studies restricted the energy range to be greater than 1 GeV to limit the contamination. However, this criterion is only valid in stacking the brightest sources and analyzing their angular photon distribution. While HSP BL Lacs are the most likely halo sources, they are not the brightest sources for Fermi-LAT. Moreover, the containment angle of the PSF at 1 GeV is ∼1°, large enough to still allow contamination from nearby sources for many of these AGNs.

The nondetection of the signal in our higher energy bins potentially indicates a low spectral intensity of cascade emission at higher energies. However, the energy dependence of the halo fraction $f_{\rm halo}$ is a function of the cascade and intrinsic spectra, which cannot be directly detected and depends on detailed knowledge of the AGN jet, EBL, IGMF, and the pair cooling processes. At present, lacking knowledge of those processes or a precise measurement of the source spectra, we cannot draw any solid conclusion about the energy dependence of the pair halo, especially for a set of sources with different spectra.

Given the limitations of the stacking-source method, only an average range of the IGMFs can be recovered. In a finite sky region, the emission from very large halos will be taken into account in our statistical analysis as background counts, because our method is insensitive to very large pair halos, whose photon fluxes are too extended to be resolved from the background emission. Since the maximum angular search window is limited by source confusion and other experimental factors, we cannot provide as strong a constraint on the maximum allowed angular extent of the GeV γ-ray emission and the maximum field strength as we can on the minimum angular extent and field strength (as shown in Fig. 3, where a long tail of significance can be seen at large angles). In addition, the small-angle approximation implicit in Eq. (1) might not hold for the larger magnetic fields, since the electron-positron pairs might follow trajectories with complete loops [36]. Thus, the estimation of IGMFs in this study is still marginally consistent with the results from Tashiro *et al.* [37], in which the strength of the helical component of the IGMF is given as $\sim 10^{-14}$ G by analyzing the Fermi extragalactic diffuse background.

Further data, including improved observations by Fermi and new data from forthcoming instruments, should be analyzed to put our findings on firmer ground. We hope that better spatial and spectral resolution of the pair halos will enable a detailed story of the IGMF to emerge.

The authors acknowledge the Fermi team for providing the Fermi-LAT data (available in the Fermi Science Support Center, http://fermi.gsfc.nasa.gov/ssc/). W. C. thanks the Department of Physics, Washington University in St. Louis (WUSTL) for the Arthur L. Hughes Fellowships to support his study. J. H. B. and F. F. have been partially supported by the U.S. Department of Energy Grant No. DE-FG02-91ER40628 at WUSTL.

*wenleichen@wustl.edu

[1] A. Kandus, K. E. Kunze, and C. G. Tsagas, Phys. Rep. **505**, 1 (2011).
[2] R. Durrer and A. Neronov, Astron. Astrophys. Rev. **21**, 62 (2013).
[3] P. L. Nolan *et al.*, Astrophys. J. Suppl. Ser. **199**, 31 (2012).
[4] M. Ackermann *et al.*, Astrophys. J. Suppl. Ser. **209**, 34 (2013).
[5] A. Furniss, D. A. Williams, C. Danforth, M. Fumagalli, J. X. Prochaska, J. Primack, C. M. Urry, J. Stocke, A. V. Filippenko, and W. Neely, Astrophys. J. **768**, L31 (2013).
[6] F. Aharonian, W. Essey, A. Kusenko, and A. Prosekin, Phys. Rev. D **87**, 063002 (2013).
[7] W. Essey and A. Kusenko, Astropart. Phys. **33**, 81 (2010).
[8] W. Essey, O. E. Kalashev, A. Kusenko, and J. F. Beacom, Phys. Rev. Lett. **104**, 141102 (2010).
[9] W. Essey, O. E. Kalashev, A. Kusenko, and J. F. Beacom, Astrophys. J. **731**, 51 (2011).
[10] W. Essey and A. Kusenko, Astrophys. J. **751**, L11 (2012).
[11] S. Ando and A. Kusenko, Astrophys. J. **722**, L39 (2010).
[12] A. Neronov, D. V. Semikoz, P. G. Tinyakov, and I. I. Tkachev, Astron. Astrophys. **526**, A90 (2011).
[13] A. A. Abdo *et al.*, Astropart. Phys. **32**, 193 (2009).
[14] M. Ackermann *et al.*, Astrophys. J. **765**, 54 (2013).
[15] K. Murase, K. Takahashi, S. Inoue, K. Ichiki, and S. Nagataki, Astrophys. J. **686**, L67 (2008).
[16] A. Neronov and I. Vovk, Science **328**, 73 (2010).
[17] W. Essey, S. Ando, and A. Kusenko, Astropart. Phys. **35**, 135 (2011).
[18] T. C. Arlen, V. V. Vassiliev, T. Weisgarber, S. P. Wakely, and S. Y. Shafi, Astrophys. J. **796**, 18 (2014).
[19] Y. T. Tanaka *et al.*, Astrophys. J. **787**, 155 (2014).
[20] A. Neronov and D. V. Semikoz, Phys. Rev. D **80**, 123012 (2009).
[21] See Supplemental Material at http://link.aps.org/supplemental/10.1103/PhysRevLett.115.211103, which includes Refs. [22–26], for details of the data selection methods, derivations of Eq. 1, and details of the statistical analysis.
[22] http://fermi.gsfc.nasa.gov/ssc/data/access/lat/BackgroundModels.html.
[23] H. Jeffreys, *Theory of Prabability*, 3rd ed. (Oxford University Press, Oxford, 1961).
[24] S. S. Wilks, Ann. Math. Stat. **9**, 60 (1938).
[25] M. J. D. Powell, Computer Journal (UK) **7**, 155 (1964).
[26] J. R. Mattox *et al.*, Astrophys. J. **461**, 396 (1996).
[27] http://www-glast.slac.stanford.edu/software/IS/glast_lat_performance.htm.
[28] H. Tashiro and T. Vachaspati, Phys. Rev. D **87**, 123527 (2013).
[29] G. Ghisellini, A. Celotti, G. Fossati, L. Maraschi, and A. Comastri, Mon. Not. R. Astron. Soc. **301**, 451 (1998).
[30] G. Fossati, L. Maraschi, A. Celotti, A. Comastri, and G. Ghisellini, Mon. Not. R. Astron. Soc. **299**, 433 (1998).
[31] M. Ackermann *et al.*, Astrophys. J. **726**, 35 (2011).
[32] J. J. Hester, Annu. Rev. Astron. Astrophys. **46**, 127 (2008).
[33] S. A. Baldwin and G. W. Fellingham, Psychol. Methods **18**, 151 (2013).
[34] R. E. Kass and A. E. Raftery, J. Am. Stat. Assoc. **90**, 773 (1995).
[35] R. Protassov, D. A. van Dyk, A. Connors, V. L. Kashyap, and A. Siemiginowska, Astrophys. J. **571**, 545 (2002).
[36] We thank A. Long and T. Vachaspati for this remark.
[37] H. Tashiro, W. Chen, F. Ferrer, and T. Vachaspati, Mon. Not. R. Astron. Soc. **445**, L41 (2014).